



# Phase diagram studies for the growth of (Mg,Zr):SrGa<sub>12</sub>O<sub>19</sub> crystals

Detlef Klimm<sup>1</sup> · Bartosz Szczefanowicz<sup>1,2,3</sup> · Nora Wolff<sup>1,4</sup> · Matthias Bickermann<sup>1</sup>

Received: 1 December 2020 / Accepted: 21 August 2021  
© The Author(s) 2021

## Abstract

By differential thermal analysis, a concentration field suitable for the growth of Zr, Mg co-doped strontium hexagallate crystals was observed that corresponds well with known experimental results. It was shown that the melting point of doped crystal is ca. 60 K higher than that of undoped crystals. This higher melting points indicate hexagallate phase stabilization by Zr, Mg co-doping and increase the growth window of (Mg,Zr):SrGa<sub>12</sub>O<sub>19</sub>, compared to undoped SrGa<sub>12</sub>O<sub>19</sub> that grows from SrO–Ga<sub>2</sub>O<sub>3</sub> melts.

**Keywords** Hexaferrite structure · Thermal analysis · Phase diagram · Metastability · Crystal growth

## Introduction

Among the many pseudobinary compounds in the system SrO–Ga<sub>2</sub>O<sub>3</sub>, the composition of SrGa<sub>12</sub>O<sub>19</sub> is closest to the component GaO<sub>1.5</sub> = ½ Ga<sub>2</sub>O<sub>3</sub>, with a molar fraction of GaO<sub>1.5</sub>,  $x = 0.9231$  (Table 1). SrGa<sub>12</sub>O<sub>19</sub> is isostructural to the mineral magnetoplumbite, (Pb,Mn<sup>2+</sup>,Mg<sup>2+</sup>)(Fe<sup>3+</sup>,Mn<sup>3+</sup>)<sub>12</sub>O<sub>19</sub>, space group *P6<sub>3</sub>/mmc*, which again belongs to the larger group of hexagonal ferrites, or “hexaferrites” [1]. Many of these materials possess strong and highly anisotropic persistent magnetic and electric moments, which make them interesting as permanent magnets or even multiferroics. Crystal growth of Fe<sup>3+</sup> based hexaferrites is a challenge, because at the high melting points beyond 1500 °C of these materials, partial reduction to Fe<sup>2+</sup> occurs; typically, liquidus temperatures are reduced by foreign solvents like Na<sub>2</sub>O to stabilize iron valency [2]. Resulting from the structural similarity, SrGa<sub>12</sub>O<sub>19</sub> is a good substrate crystal for the epitaxial deposition of other hexaferrites [3].

Moreover, the chemical versatility of the magnetoplumbite structure allows doping of SrGa<sub>12</sub>O<sub>19</sub> with luminescent ions such as Mn<sup>2+</sup> and Cr<sup>3+</sup> [4, 5].

The first publication of a phase diagram for the system SrO–Ga<sub>2</sub>O<sub>3</sub> [6] showed that SrGa<sub>2</sub>O<sub>4</sub> is the only intermediate compound with a congruent melting point. In more recent studies, this system was redetermined and partially thermodynamically assessed [7, 8], with mainly similar results like the previous study [6] – but with the difference that the peritectic melting of SrGa<sub>12</sub>O<sub>19</sub> was reported there at significantly higher temperature (Table 1). However, all studies agree with the observation that it melts peritectically with the formation of β-Ga<sub>2</sub>O<sub>3</sub>. A somewhat lower peritectic melting temperature 1540 °C for SrGa<sub>12</sub>O<sub>19</sub> and 1530 °C for BaGa<sub>12</sub>O<sub>19</sub> was reported elsewhere; both compounds form an isomorph solid solution series [9, 10]. For the SrO–Ga<sub>2</sub>O<sub>3</sub> system, minor differences are reported mainly on the SrO side, the reader is referred to the PhD theses of Solak [11] and Richter [12].

As a result of peritectic melting, crystal growth of SrGa<sub>12</sub>O<sub>19</sub> is only possible from melts with an excess of SrO, compared to the stoichiometry of the compound. According to the assessment of Zinkevich [8], this phase with a Ga<sub>2</sub>O<sub>3</sub> molar fraction  $x = 0.9231$  is in equilibrium with the melt only between the peritectic points of SrGa<sub>12</sub>O<sub>19</sub> ( $x^{\text{per}} = 0.8002$ ,  $T^{\text{per}} = 1553$  °C) and the neighboring phase SrGa<sub>4</sub>O<sub>7</sub> ( $x^{\text{per}} = 0.7723$ ,  $T^{\text{per}} = 1492$  °C). (The concentration data from [8] that are based on the components SrO and Ga<sub>2</sub>O<sub>3</sub> were converted to SrO and GaO<sub>1.5</sub> which are used here.) With the lever rule, from these data a maximum

✉ Detlef Klimm  
detlef.klimm@ikz-berlin.de

<sup>1</sup> Leibniz-Institut für Kristallzüchtung, Max-Born-Str. 2,  
12489 Berlin, Germany

<sup>2</sup> Institute of Physics, Poznan University of Technology,  
Piotrowo 3, 60-965 Poznan, Poland

<sup>3</sup> Present Address: INM – Leibniz Institute for New Materials,  
Campus D2 2, 66123 Saarbrücken, Germany

<sup>4</sup> Present Address: Helmholtz-Zentrum für Materialien und  
Energie, Hahn-Meitner-Platz 1, 14109 Berlin, Germany

**Table 1** Compounds in the pseudobinary system (1 - x) SrO - x GaO<sub>1.5</sub>

Formula	x	Remarks and reference
SrO	0.0000	$T_f = 2665$ °C congruent [18]
Sr <sub>4</sub> Ga <sub>2</sub> O <sub>7</sub>	0.3333	$T_f = 1540$ °C [7], or 1476 °C [6] peritectic
Sr <sub>7</sub> Ga <sub>4</sub> O <sub>13</sub>	0.3636	$T_f = 1490$ °C [7] peritectic, not found here
Sr <sub>10</sub> Ga <sub>6</sub> O <sub>19</sub>	0.3750	structure reported from [19, 20]
Sr <sub>3</sub> Ga <sub>2</sub> O <sub>6</sub>	0.4000	$T_f = 1230$ °C [7] peritectoid
Sr <sub>3</sub> Ga <sub>4</sub> O <sub>9</sub>	0.5714	$T_f = 1350$ °C [7], or 1322 °C [6] peritectic
SrGa <sub>2</sub> O <sub>4</sub>	0.6667	$T_f = 1430$ °C, $T_i = 1550$ °C [7], or 1580 °C [6] congruent
SrGa <sub>4</sub> O <sub>7</sub>	0.8000	$T_f = 1490$ °C [7], or 1422 °C [6] peritectic
SrGa <sub>12</sub> O <sub>19</sub>	0.9231	$T_f = 1550$ °C [7], 1553 °C [8], or 1462 °C [6] peritectic
Ga <sub>2</sub> O <sub>3</sub>	1.0000	$T_f = 1800$ °C congruent [18]

$T_f$  marks congruent or peritectic melting points, or peritectoid decomposition temperatures.  $T_i$  are transition temperatures between different phases of one compound. For structural data of these compounds see, e.g., Ropp [17]

yield  $Y = (0.8002 - 0.7723)/(0.9231 - 0.7723) \approx 18\%$  for the growth of SrGa<sub>12</sub>O<sub>19</sub> crystals from melts with excess SrO can be calculated.

First SrGa<sub>12</sub>O<sub>19</sub> crystals with size up to 3 mm were grown by Haberey et al. [13] from fluxes with  $x = 0.830$ , which means a slightly higher GaO<sub>1.5</sub> concentration than the peritectic point given by Zinkevich [8],  $x^{\text{per}} = 0.8002$ . This difference indicates that supercooling of the melt might avoid the primary crystallization of  $\beta$ -Ga<sub>2</sub>O<sub>3</sub>. Later, the same authors performed growth experiments with the addition of alkali molybdates or bismuth oxide. From melt solutions with Bi<sub>2</sub>O<sub>3</sub> as flux, SrGa<sub>12</sub>O<sub>19</sub> crystals up to 15 mm diameter (useful area up to 30 mm<sup>2</sup>) could be obtained. However, these crystals incorporated ca. 0.5 mol% Bi [14].

Significantly better and larger crystals were obtained by Mateika and Laurien [15]. They stated that the small concentration region in the pseudobinary system where SrGa<sub>12</sub>O<sub>19</sub> crystallizes first (in their paper  $0.7730 \leq x(\text{GaO}_{1.5}) \leq 0.8095$ , very similar to the data given above) can be increased, if Ga<sup>3+</sup> is substituted partially by small equimolar additions of Mg<sup>2+</sup> and Zr<sup>4+</sup>. The partitioning coefficients of both ions was found to be  $k \approx 1.05 > 1$ , which suggest that the hexaferrite structure is stabilized. The possibility to substitute Ga<sup>3+</sup> by equimolar amounts of Mg<sup>2+</sup> and Zr<sup>4+</sup> was already earlier demonstrated for Gd<sub>3</sub>Ga<sub>5</sub>O<sub>12</sub> [16].

## Experimental

Differential thermal analysis (DTA) with simultaneous thermogravimetry (TG) was performed using NETZSCH STA 449C “Jupiter” and STA 409CD thermal analyzers. DTA/TG sample holders with Pt/Pt90Rh10 thermocouples and lidded platinum crucibles allowed measurements up to 1650 °C in a flowing mixture of 20 mL min<sup>-1</sup> Ar + 20 mL min<sup>-1</sup> O<sub>2</sub>. (Ga<sub>2</sub>O<sub>3</sub> evaporates mainly under dissociation as Ga<sub>2</sub>O, and SrO mainly

as metallic Sr; and both reactions can be suppressed by adding O<sub>2</sub> to the atmosphere.) Usually the DTA samples were molten twice to ensure good mixing, and the second heating curves were used for further analysis. Unfortunately, under these experimental conditions the liquidus temperatures of mixtures close to the high melting components SrO and Ga<sub>2</sub>O<sub>3</sub> (cf. Table 1) cannot be accessed, which prohibits good mixing and equilibration of DTA samples. Alternative DTA setups with higher maximum temperature cannot be used, because sample holder and/or furnaces contain parts that are sensitive with respect to oxygen (e.g., from tungsten or graphite). Under reducing conditions, however, both components are prone to decomposition to metallic Sr or Ga, or Ga<sub>2</sub>O suboxide, respectively, and subsequent evaporation. Ca. 50 different compositions spanning the whole range from pure SrO to pure Ga<sub>2</sub>O<sub>3</sub> were prepared by melting together appropriate quantities of SrCO<sub>3</sub> and Ga<sub>2</sub>O<sub>3</sub> powders (Alfa, 99.99% purity) in the DTA crucibles.

Prior to charging the samples into the DTA crucibles, the starting materials were checked for mass losses by emanating CO<sub>2</sub> (from carbonate calcination) or adsorbed volatiles such as traces of water. The samples themselves, with masses of at least 50 mg, were prepared on a balance with 0.01 mg resolution. This high accuracy ensures that concentration errors are insignificant.

In a second series MgO, ZrO<sub>2</sub>, and an equimolar mixture of MgO + ZrO<sub>2</sub> was added to a (1 - x) SrO + x GaO<sub>1.5</sub> mixture with  $x = 0.857$ , that is close to the growth window of SrGa<sub>12</sub>O<sub>19</sub>. Only MgO + ZrO<sub>2</sub> co-doping proved to be useful. It was the aim of this series to reveal the influence of these dopants on the growth window.

## Results and discussion

As mentioned in the previous section, the liquidus temperatures close to pure strontium or gallium oxide, respectively, are so high that evaporation from the sample prevents reliable thermal analysis. Not so in the center of the system where a low eutectic (1326 °C,  $x=0.49$ ) between Sr<sub>10</sub>Ga<sub>6</sub>O<sub>19</sub> and Sr<sub>3</sub>Ga<sub>4</sub>O<sub>9</sub> results in low liquidus temperatures without significant evaporation (cf. Fig. 2). Nevertheless, another peculiarity made interpretation of DTA signals not straightforward there: It turned out that DTA curves were often not well reproducible, especially for

compositions from the central region of the phase diagram. This is demonstrated for  $(1-x)$  SrO +  $x$  GaO<sub>1.5</sub> mixtures with  $x=0.5549$  (two subsequent heatings of one sample) and  $x=0.5855$  (three heatings) in Fig. 1.

It is obvious that the curve (1) for sample  $x=0.5549$ , and curves (2) and (3) for sample  $x=0.5855$  show exothermal peaks during these heating runs, which is untypical. All melting processes are endothermal events, but exothermal effects may occur if a sample is not in thermodynamic equilibrium and returns to equilibrium during heating.

For the  $x=0.5549$  sample, the peaks with onsets at 1241 °C and 1326 °C appear for both heating runs, because there equilibrium is obviously obtained, also for the upper

**Fig. 1** Subsequent DTA heating curves for identical samples with  $x=0.5549$  (top two curves) or  $x=0.5855$  (bottom three curves), respectively. Occasional exothermal peaks result from non-equilibrium that was obtained during previous cooling

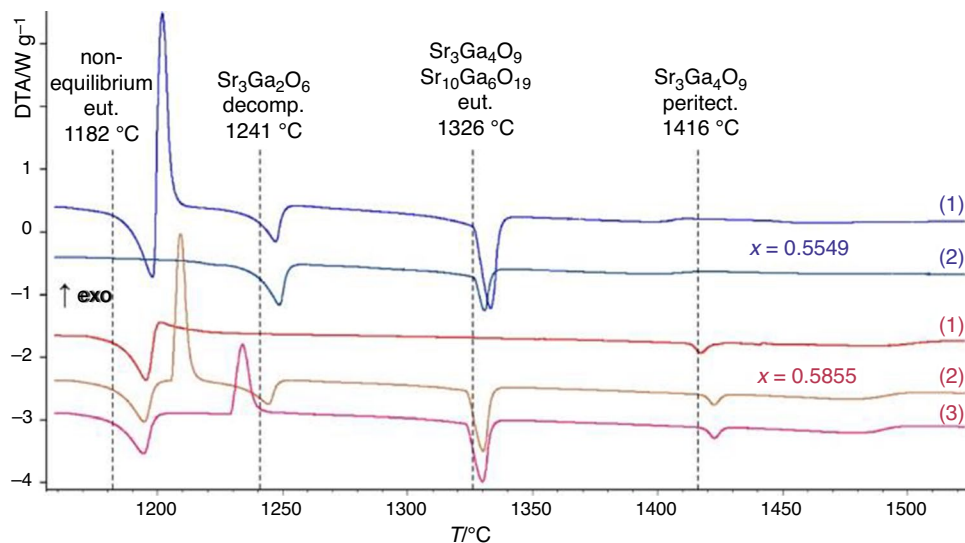
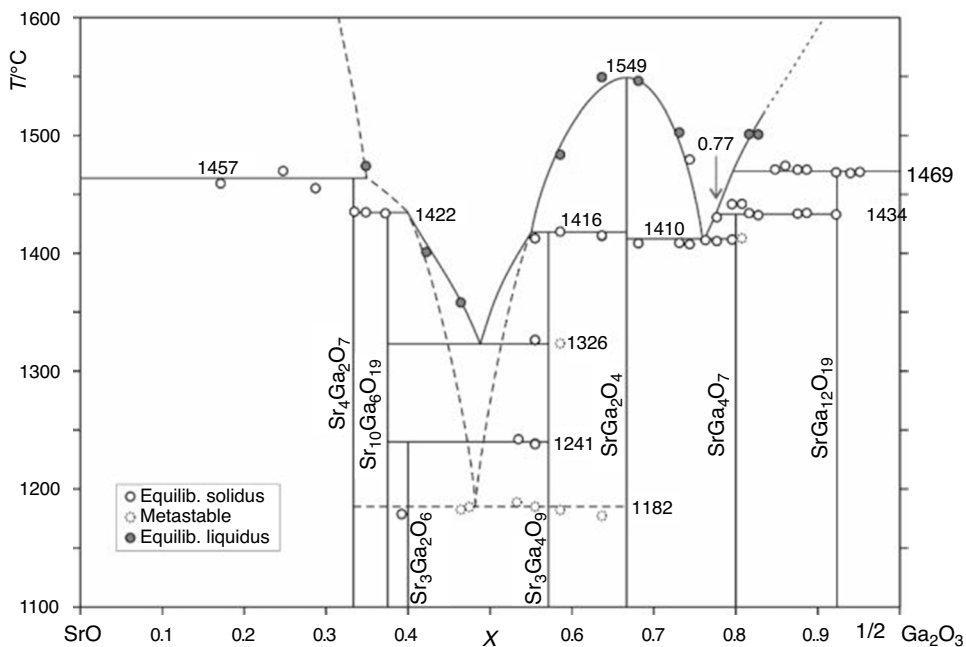


**Fig. 2** Experimental phase diagram Ga<sub>2</sub>O<sub>3</sub>-SrO with seven intermediate compounds. Only a part of the experimental points is shown. Dashed liquidus lines indicate strong evaporation resulting from high temperatures close to the end members, or metastability near  $x=0.5$ , respectively. Besides, one metastable eutectic at 1182 °C is drawn



curve. Not so the peak with onset at 1182 °C which results from a non-equilibrium situation. From Fig. 2 it can be seen that this could be possible, e.g., if  $\text{Sr}_3\text{Ga}_4\text{O}_9$  as well as  $\text{Sr}_3\text{Ga}_2\text{O}_6$  are not formed. This can occur as a result of strong supercooling of both phases, which results in the non-equilibrium crystallization of their neighbors  $\text{SrGa}_2\text{O}_4$  and  $\text{Sr}_{10}\text{Ga}_6\text{O}_{19}$ . Then, however, it is normal that these neighbor phases form together a lower eutectic (indicated by the dashed isotherm at 1182 °C and the non-equilibrium prolongations of the liquidus lines in Fig. 2).

Curve (1) for the  $x=0.5855$  sample shows the same non-equilibrium eutectic. No other effects appear until 1416 °C, which is the peritectic melting temperature of  $\text{Sr}_3\text{Ga}_4\text{O}_9$ . This melting temperature was found here higher than reported in recent studies [6, 12], but we assume that these authors mixed up the eutectic at 1326 °C with the peritectic melting of  $\text{Sr}_3\text{Ga}_4\text{O}_9$ . It should be noted that the composition of this sample is just 1.4% right from  $\text{Sr}_3\text{Ga}_4\text{O}_9$ , and hence this phase should be predominating there under equilibrium conditions. Only in curve (2) of this sample,  $\text{Sr}_3\text{Ga}_2\text{O}_6$  is formed as a non-equilibrium phase first, which decomposes soon at 1241 °C to  $\text{Sr}_3\text{Ga}_4\text{O}_9$  and  $\text{Sr}_{10}\text{Ga}_6\text{O}_{19}$ , which then melt eutectically at 1326 °C. The last heating curve (3) for this sample is similar to the previous one—with the difference that the exothermal jump into equilibrium occurs slightly later, and consequently the decomposition peak of  $\text{Sr}_3\text{Ga}_2\text{O}_6$  cannot be observed.

After passing all DTA peaks, the  $x=0.5855$  curves show an upward bend near 1490 °C. This indicates the liquidus temperature at this composition, because all melting processes are completed and the DTA curves return to their basis line. For the  $x=0.5549$  sample an analogous (but weaker) bend occurs near 1400 °C because this composition is closer to the eutectic point. However, for this experimental point, drawn slightly below the left termination of the 1416 °C peritectic in Fig. 2, this peritectic and the liquidus of  $\text{Sr}_3\text{Ga}_4\text{O}_9$  as well as  $\text{SrGa}_2\text{O}_4$ , cannot be resolved experimentally.

A tentative phase diagram of the system  $\frac{1}{2}\text{Ga}_2\text{O}_3\text{--SrO}$  is shown in Fig. 2 which is partially based on the references [6, 7, 10–12], but complemented and corrected with experimental DTA points from this study. It is obvious that not all experimental points can be explained by the liquidus and isothermal lines in the diagram. However, additional non-equilibrium events can be expected to occur, e.g., if one or two of the equilibrium eutectic phases at 1326 °C are absent. Other effects, like the peaks on the 1410 °C level right from  $x=0.8$ , result from the initial crystallization of the hexagallate  $\text{SrGa}_{12}\text{O}_{19}$ , which shifts the concentration of the rest melt to the left. The remaining melt is depleted by  $\text{Ga}_2\text{O}_3$  and its composition moves along the liquidus toward the eutectic point near  $x=0.76$ , which produces then the corresponding peak also for compositions right from  $\text{SrGa}_4\text{O}_7$ .

The occurrence of metastable non-equilibrium near the eutectic composition agrees with X-ray measurements and optical microscopy by Batti & Slocchari [6] who observed repeatedly  $\text{Sr}_4\text{Ga}_2\text{O}_7$  for such samples—which contradicts thermodynamic equilibrium. The large endothermal effect at 1182 °C (cf. also Fig. 1) is interpreted in Fig. 2 as metastable eutectic between  $\text{Sr}_4\text{Ga}_2\text{O}_7$  and  $\text{SrGa}_2\text{O}_4$ . However, this interpretation is not assured, because the inclusion of other phases (e.g.,  $\text{Sr}_3\text{Ga}_2\text{O}_6$ ) cannot be ruled out.

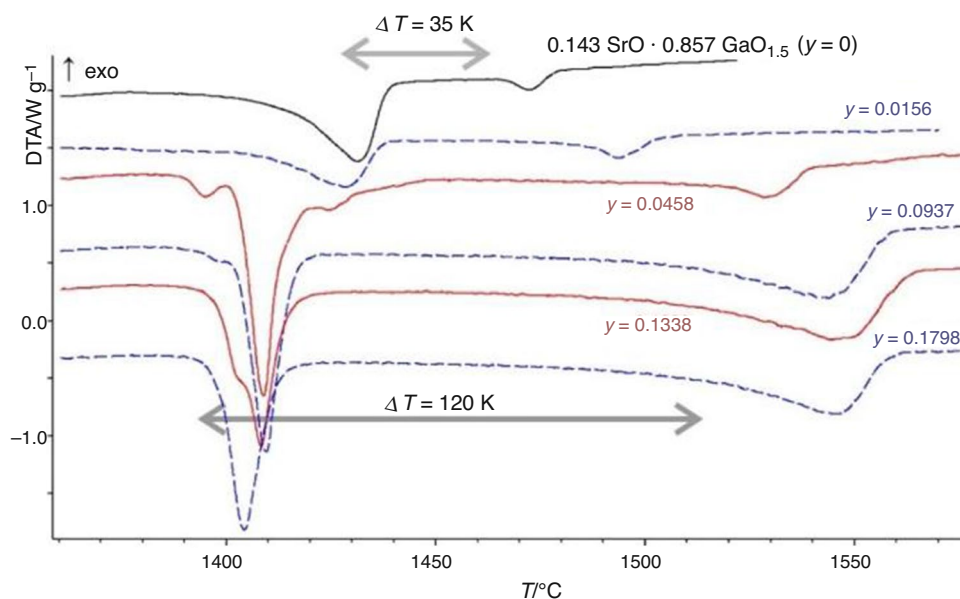
In agreement with the Mateika & Laurien paper [15], Fig. 2 shows that the  $\text{SrGa}_{12}\text{O}_{19}$  liquidus, and hence its crystallization window, is extremely narrow. Moreover, crystal growth is hampered there by the non-equilibrium crystallization of the neighbor phase  $\text{SrGa}_4\text{O}_7$  [15]. As pointed out before, the occasional crystallization of non-equilibrium phases seems to be a general issue of the  $\text{Ga}_2\text{O}_3\text{--SrO}$  system.

In the magnetoplumbite crystal structure, the  $\text{Ga}^{3+}$  ions reside in octahedral, bipyramidal, and tetragonal environments, and the fivefold coordinated  $\text{Ga}^{3+}$  is randomly displaced from the center of its trigonal bipyramidal coordination polyhedron along positive and negative directions of the  $c$ -axis [1, 21, 22]. Mateika & Laurien [15] succeeded to increase the growth window of  $\text{SrGa}_{12}\text{O}_{19}$  by partial substitution of  $\text{Ga}^{3+}$  (ionic radius  $r$  [6] = 76;  $r$  [4] = 61 pm [23]) by simultaneous substitution with identical amounts of  $\text{Mg}^{2+}$  ( $r$  [6] = 86;  $r$  [4] = 71 pm) and  $\text{Zr}^{4+}$  ions ( $r$  [6] = 86;  $r$  [4] = 73 pm), and crystals > 1 cm<sup>3</sup> could be grown from a  $\text{Sr}_{1.56}\text{Ga}_{10.40}\text{Mg}_{0.52}\text{Zr}_{0.52}\text{O}_{18.72}$  melt [15].

It was the purpose of further DTA measurements in this study to investigate how  $\text{Mg}^{2+}$  and/or  $\text{Zr}^{4+}$  doping influences relevant phase equilibria in the  $\frac{1}{2}\text{Ga}_2\text{O}_3\text{--SrO}$  system. From Fig. 2 it is evident that crystal growth of  $\text{SrGa}_{12}\text{O}_{19}$  should be possible along its liquidus between the peritectic lines at 1469 °C and 1434 °C, which is a very narrow growth window. In three series of DTA measurements, to a  $\text{SrO/Ga}_2\text{O}_3$  mixture with  $x=0.8571$  (where both peritectic peaks are strong) growing amounts of  $\text{MgO}$  only,  $\text{ZrO}_2$  only, and of an equimolar  $\text{MgO/ZrO}_2$  mixture were added.

Doping by exclusively  $\text{MgO}$  or  $\text{ZrO}_2$  was not useful: In both cases the 1434 °C peak ( $\text{SrGa}_4\text{O}_7$  peritectic) is lowered by 10 K, but the 1469 °C peak ( $\text{SrGa}_{12}\text{O}_{19}$  peritectic) disappeared for additive levels around 4%—indicating instability of the hexagallate phase. Not so for equimolar  $\text{MgO/ZrO}_2$  doping, which is shown in Fig. 3. It turns out that again the lower peritectic moves downward, here by 20 K. Even more impressing is that the higher peritectic, which is the upper stability range of the hexagallate phase, shifts by > 60 K upward. As already pointed out by Mateika & Laurien [15], obviously the co-doping with  $\text{Mg}^{2+}/\text{Zr}^{4+}$  increases the stability range. One can see from Fig. 3 that an upper useful co-doping level, is of the order  $y=0.1$ , where  $y$  is the mole fraction of  $(\text{MgO} + \text{ZrO}_2)$  per 1 mol of  $\text{SrGa}_{12}\text{O}_{19}$ . This means each 10% of  $\text{MgO}$  and  $\text{ZrO}_2$  can be added. One can

**Fig. 3** Starting from a  $(1-x)$  SrO +  $x$  GaO<sub>1.5</sub> mixture with  $x=0.857$  (cf. Fig. 2), growing molar concentrations  $y$  of a MgO:ZrO<sub>2</sub> = 1:1 mixture were added. This increases the difference between the lower SrGa<sub>4</sub>O<sub>7</sub> and the higher SrGa<sub>12</sub>O<sub>19</sub> peritectic decomposition significantly



assume that the highly versatile coordinations [4–6] of Ga<sup>3+</sup> in the hexaferrite structure support the partial replacement of this ion by the Mg<sup>2+</sup>/Zr<sup>4+</sup> dopant. Besides, the high number of four components leads at liquidus temperatures around 1500 °C to a significant entropic stabilization of the (Mg, Zr):SrGa<sub>12</sub>O<sub>19</sub> mixture phase.

The graphical representation of this co-doping is not straightforward, because quaternary systems cannot be drawn without constraints in two dimensions. Mateika & Laurien [15] used a simplified concentration triangle with (MgO:ZrO<sub>2</sub>)–Ga<sub>2</sub>O<sub>3</sub>–SrO as pseudocomponents or components, respectively. This is reasonable, because MgO and

ZrO<sub>2</sub> are used only in the 1:1 molar ratio, and it is justified, because only the rim systems SrO–Ga<sub>2</sub>O<sub>3</sub>, SrO–ZrO<sub>2</sub>, and MgO–Ga<sub>2</sub>O<sub>3</sub> are relevant for the discussion. Figure 4 a) is a similar presentation of this concentration triangle, with the difference that 1/2Ga<sub>2</sub>O<sub>3</sub> and 1/2(MgO:ZrO<sub>2</sub>) are defined as components. This has the benefit that all corners represent one single cation.

The further discussion may neglect the potential rim system MgO–SrO because this is simple eutectic without intermediate compounds, and hence no other phases that could crystallize first [24]. The other potential rim system ZrO<sub>2</sub>–Ga<sub>2</sub>O<sub>3</sub> is not known from the literature. However,

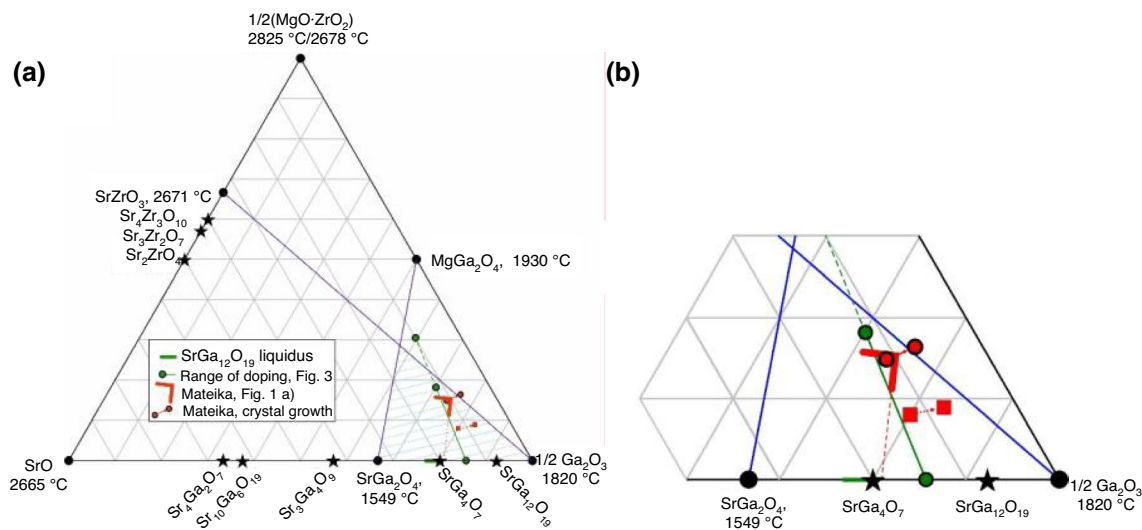


**Fig. 4** **a** Concentration triangle SrO–1/2 Ga<sub>2</sub>O<sub>3</sub>–1/2 (MgO:ZrO<sub>2</sub>). Compounds with congruent melting points are marked by circles ●, with peritectic melting by asterisks ★. Blue tie lines SrZrO<sub>3</sub>–Ga<sub>2</sub>O<sub>3</sub> and

MgGa<sub>2</sub>O<sub>4</sub>–SrGa<sub>2</sub>O<sub>4</sub> separate independent partial systems. Data of Mateika & Laurien [15] and from this study added. **b** Ga<sub>2</sub>O<sub>3</sub> rich corner of the triangle

simple Ga-Zr oxides do not exist and Ga–O–Zr bonds can be stabilized only with organic ligands [25]. Hence, one can assume that also the  $\text{ZrO}_2\text{–Ga}_2\text{O}_3$  system is eutectic, like  $\text{ZrO}_2\text{–Al}_2\text{O}_3$  [26]. Indeed, from  $\text{Ga}_2\text{O}_3$  rich ternary melts with high  $\text{MgO/ZrO}_2$  doping only  $\text{MgGa}_2\text{O}_4$  crystallized in addition to  $\text{SrGa}_{12}\text{O}_{19}$  and  $\beta\text{-Ga}_2\text{O}_3$ , and no Ga-Zr oxide phase was found [15]. Consequently, also the potential rim system  $\text{ZrO}_2\text{–Ga}_2\text{O}_3$  can be neglected.

Both remaining rim systems that include  $\text{MgO}\cdot\text{ZrO}_2$  contain one intermediate compound with congruent melting behavior:  $\text{SrZrO}_3$  ( $T_f=2671\text{ }^\circ\text{C}$ , [27]) and  $\text{MgGa}_2\text{O}_4$  ( $T_f\approx 1930\text{...}1950\text{ }^\circ\text{C}$ , [28, 29]). If intermediate compounds in ternary systems can coexist in equilibrium, tie lines can be drawn between them and the concentration triangle can be divided to partial systems. It is very common that such tie lines can be drawn between congruently melting phases, although exceptions are possible, e.g., near ternary peritectic points [30]. In such cases, however, three solid phases should coexist, which was not reported in the literature [15, 31] so far.

Figure 4 a shows the concentration triangle with these tie lines that separate independent partial systems. The considerations given above allow to conclude that for melts inside the shaded area, the whole crystallization path remains within this triangle, because this is a partial system. The triangle is enlarged in Fig. 4 b. The experiments by Mateika & Laurien resulted in the red corner as upper useful limits for the  $\text{Ga}_2\text{O}_3$  and dopant concentrations (in reference [15] Fig. 1 a. In this publication, the chemical composition of melts was compared with the composition of  $(\text{Mg,Zr})\text{:SrGa}_{12}\text{O}_{19}$  crystals that were grown, and enrichment of the dopants in the crystal was found. Besides, the peritectic melting behavior of  $\text{SrGa}_{12}\text{O}_{19}$  requires melts with a smaller  $\text{Ga}_2\text{O}_3$  concentration than the crystal. As a consequence, an upward right shift of the crystal compositions compared to the melts was observed [15].

Unfortunately, there is a contradiction: Fig. 1 in [15] shows that  $(\text{Mg,Zr})\text{:SrGa}_{12}\text{O}_{19}$  crystallizes only from melts inside the “red corner” in Fig. 4 of this article; but the melt composition  $\text{Sr}_{1.56}\text{Ga}_{10.40}\text{Mg}_{0.52}\text{Zr}_{0.52}\text{O}_{18.72}$  that is given in Tab. 2 of the Mateika & Laurien paper corresponds to the left red square in Fig. 4, and the resulting crystal to the right square. We assume that concentration data were mixed up and can only guess that dopant concentration have to be doubled. Then the melt concentration lies almost exactly in the corner, and the result is (within the typical experimental error) almost exactly on the blue rim of the partial triangle. One can conclude that by trial and error Mateika & Laurien found a melt composition that is almost optimum for crystal growth in this system.

The DTA measurements that are shown in Fig. 3 are a confirmation: The growth window for  $(\text{Mg,Zr})\text{:SrGa}_{12}\text{O}_{19}$  could be increased mainly by an increased stability of

hexagallate phase. This works well up to the  $y=0.0937$  doping level. The starting composition of this doping series,  $x=0.857$ , and the useful upper doping level are marked by green circles in Fig. 4. Higher doping along the green dashed line is detrimental because the partial system is left.

## Conclusions

Mateika & Laurien [15] identified a concentration field in the quaternary system  $\text{SrO}\text{–Ga}_2\text{O}_3\text{–MgO}\text{–ZrO}_2$  where the growth of bulk  $(\text{Mg,Zr})\text{:SrGa}_{12}\text{O}_{19}$  crystals is possible. With DTA measurements, this concentration field was confirmed to be optimum, and a further optimization with respect to starting composition seems not possible. One technical error concerning concentration data in Tab. 2 of [15] was identified.

**Acknowledgements** The authors thank Christo Gugushev for helpful discussions on this topic, and Steffen Ganschow for hints improving the manuscript. B.S. acknowledges support from the EU in the framework of the Erasmus+ program.

**Author contributions** All authors contributed to the study conception and design. Material preparation, data collection and analysis were performed by B.S. The first draft of the manuscript was written by DK and all authors commented on previous versions of the manuscript. All authors read and approved the final manuscript.

**Funding** Open Access funding enabled and organized by Projekt DEAL.

**Open Access** This article is licensed under a Creative Commons Attribution 4.0 International License, which permits use, sharing, adaptation, distribution and reproduction in any medium or format, as long as you give appropriate credit to the original author(s) and the source, provide a link to the Creative Commons licence, and indicate if changes were made. The images or other third party material in this article are included in the article's Creative Commons licence, unless indicated otherwise in a credit line to the material. If material is not included in the article's Creative Commons licence and your intended use is not permitted by statutory regulation or exceeds the permitted use, you will need to obtain permission directly from the copyright holder. To view a copy of this licence, visit <http://creativecommons.org/licenses/by/4.0/>.

## References

1. Delacotte C, Whitehead GFS, Pitcher MJ, Robertson CM, Sharp PM, Dyer MS, Alaria J, Claridge JB, Darling GR, Allan DR, Winter G, Rosseinsky MJ. Structure determination and crystal chemistry of large repeat mixed-layer hexaferrites. *IUCrJ*. 2018;5:681–98. <https://doi.org/10.1107/S2052252518011351>.
2. Gambino R, Leonhard F. Growth of barium ferrite single crystals. *J Amer Ceram Soc*. 1961;44(5):221–4. <https://doi.org/10.1111/j.1151-2916.1961.tb15364.x>.
3. Kamzin AS, Lutsev LV, Petrov VA. Epitaxial films of Ba–M type hexagonal ferrites. *Phys Solid State*. 2001;43(12):2253–6. <https://doi.org/10.1134/1.1427952>.

- Verstegen JMPJ. Luminescence of Mn<sup>2+</sup> in SrGa<sub>12</sub>O<sub>19</sub>, LaMgGa<sub>11</sub>O<sub>19</sub>, and BaGa<sub>12</sub>O<sub>19</sub>. *J Solid State Chem.* 1973;7:468–73. [https://doi.org/10.1016/0022-4596\(73\)90176-X](https://doi.org/10.1016/0022-4596(73)90176-X).
- Xu J, Chen D, Yu Y, Zhu W, Zhou J, Wang Y. Cr<sup>3+</sup>:SrGa<sub>12</sub>O<sub>19</sub>: a broadband near-infrared long-persistent phosphor. *Chem Asian J.* 2014;9:1020–5.
- Batti P, Slocchieri G. Diagramma di stato del sistema SrO–Ga<sub>2</sub>O<sub>3</sub>. *Anal Chim.* 1969;59:155–62.
- Kobzareva VP, Kovba LM, Lopato LM, Lykova LN, Shevchenko AV. Phase diagram of the system SrO–Ga<sub>2</sub>O<sub>3</sub>. *Zh Neorg Chim.* 1976;21:1651–4.
- Zinkevich M. Calorimetric study and thermodynamic assessment of the SrO–Ga<sub>2</sub>O<sub>3</sub> system. *Internat J Mat Res.* 2007;98:574–9. <https://doi.org/10.3139/146.101513>.
- Kovba LM, Lykova LN, Kobzareva VP, Lopato LM, Shevchenko AV. Phase diagram of the system BaO–Ga<sub>2</sub>O<sub>3</sub>. *Neorg Mater.* 1975;20:1970–3.
- Kadyrova ZR, Sirazhiddinov NA, Tuganova SK. Investigation of the systems SrAl<sub>12</sub>O<sub>19</sub>–Ca(Ba)Al<sub>12</sub>O<sub>19</sub> and SrGa<sub>12</sub>O<sub>19</sub>–BaGa<sub>12</sub>O<sub>19</sub>. *Neorg Mater.* 1997;33:360–3.
- Solak N. Interface stability in solid oxide fuel cells for intermediate temperature applications, Ph.D. thesis, Universität Stuttgart (2007). doi:<https://doi.org/10.18419/opus-872>.
- Richter AN, Stabilität, Kristallchemie, Strukturen und optische Eigenschaften von Hexaphasen in CaO/SrO/BaO–Al<sub>2</sub>O<sub>3</sub>/Ga<sub>2</sub>O<sub>3</sub>–MgO/MnO<sub>3</sub> Systemen, Ph.D. thesis, Friedrich-Alexander-Universität, Erlangen-Nürnberg (2012).
- Haberey F, Leckebusch R, Sahl K, Rosenberg M. Zur Züchtung von SrGa<sub>12</sub>O<sub>19</sub>-Einkristallen. *Naturwissenschaften.* 1979;66:617.
- Haberey F, Leckebusch R, Rosenberg M, Sahl K. Flux growth of SrGa<sub>12</sub>O<sub>19</sub> crystals. *J Cryst Growth.* 1983;61:284–8. [https://doi.org/10.1016/0022-0248\(83\)90364-0](https://doi.org/10.1016/0022-0248(83)90364-0).
- Mateika D, Laurien R. Czochralski growth of solid solutions of strontium hexagallate with magnesium and zirconium as dopants. *J Cryst Growth.* 1981;52:566–72. [https://doi.org/10.1016/0022-0248\(81\)90341-9](https://doi.org/10.1016/0022-0248(81)90341-9).
- Mateika D, Rusche C. Coupled substitution of gallium by magnesium and zirconium in single crystals of gadolinium gallium garnet. *J Cryst Growth.* 1977;42:440–4. [https://doi.org/10.1016/0022-0248\(77\)90229-9](https://doi.org/10.1016/0022-0248(77)90229-9).
- Ropp R.C. editor. Ch. Group 13 (B, Al, Ga, In and Tl) alkaline earth compounds. In: *Encyclopedia of the alkaline earth compounds*. Amsterdam: Elsevier;2013. pp. 481–635. <https://doi.org/10.1016/B978-0-444-59550-8.00006-5>
- [www.factsage.com](http://www.factsage.com), FactSage 7.3, GTT Technologies, Kaiserstr. 100, 52134 Herzogenrath, Germany;2019.
- Kahlenberg V. The crystal structures of the strontium gallates Sr<sub>10</sub>Ga<sub>6</sub>O<sub>19</sub> and Sr<sub>3</sub>Ga<sub>2</sub>O<sub>6</sub>. *J Solid State Chem.* 2001;160:421–9. <https://doi.org/10.1006/jssc.2001.9259>.
- Krüger H, Lazić B, Arroyabe E, Kahlenberg V. Modulated structure and phase transitions of Sr<sub>10</sub>Ga<sub>6</sub>O<sub>19</sub>. *Acta Cryst B: Struct Sci.* 2009;65:587–92. <https://doi.org/10.1107/S0108768109026974>.
- Pullar RC. Hexagonal ferrites: a review of the synthesis, properties and applications of hexaferrite ceramics. *Prog Mat Sci.* 2012;57(7):1191–310 1334. <https://doi.org/10.1016/j.pmatsci.2012.04.00>.
- Graetsch H, Gebert W. Positional and thermal disorder in the trigonal bipyramid of magnetoplumbite structure type SrGa<sub>12</sub>O<sub>19</sub>. *Z Krist Crystal Mater.* 1994;209(4):338–42. <https://doi.org/10.1524/zkri.1994.209.4.338>.
- Shannon RD. Revised effective ionic radii and systematic studies of interatomic distances in halides and chalcogenides. *Acta Cryst A.* 1976;32:751–67. <https://doi.org/10.1107/S0567739476001551>.
- van der Kemp WJM, Blok JG, van der Linde PR, Oonk HAJ, Schuijff A, Verdonk ML. Binary alkaline earth oxide mixtures: estimation of the excess thermodynamic properties and calculation of the phase diagrams. *Calphad.* 1994;18:255–67. [https://doi.org/10.1016/0364-5916\(94\)90032-9](https://doi.org/10.1016/0364-5916(94)90032-9).
- Singh S, Jancik V, Roesky HW, Herbst-Irmer R. Synthesis, characterization, and X-ray crystal structure of a gallium monohydroxide and a hetero-bimetallic gallium zirconium oxide. *Inorg Chem.* 2006;45:949–51. <https://doi.org/10.1021/ic051769i>.
- Lakiza SM, Lopato LM. Stable and metastable phase relations in the system alumina–zirconia–yttria. *J Amer Ceram Soc.* 1997;80:893–902. <https://doi.org/10.1111/j.1151-2916.1997.tb02919.x>.
- ACerS and NIST, Phase Equilibria Diagrams, V. 4.0, entry Zr-082 (2013). <https://ceramics.org/publications-resources/phaseequilibrium-diagrams>.
- Zinkevich M, Geupel S, Aldinger F. Thermodynamic assessment of the ternary systems Ga–Mg–O, Ga–Ni–O, Mg–Ni–O and extrapolation to the Ga–Mg–Ni–O phase diagram. *J Alloy Compd.* 2005;393:154–66. <https://doi.org/10.1016/j.jallcom.2004.09.069>.
- Galazka Z, Klimm D, Irmscher K, Uecker R, Pietsch M, Bertram R, Naumann M, Albrecht M, Kwasniewski A, Schewski R, Bickermann M. MgGa<sub>2</sub>O<sub>4</sub> as a new wide bandgap transparent semiconducting oxide: growth and properties of bulk single crystals. *Phys Stat Sol (a).* 2015;212:1455–60.
- Pauffer P. *Phasendiagramme*. Berlin: Akademie-Verlag; 1981.
- Majewski PJ, Rozumek M, Schluckwerder H, Aldinger F. Phase diagram studies in the systems La<sub>2</sub>O<sub>3</sub>–SrO–Ga<sub>2</sub>O<sub>3</sub>, La<sub>2</sub>O<sub>3</sub>–MgO–La<sub>2</sub>O<sub>3</sub>, and SrO–MgO–Ga<sub>2</sub>O<sub>3</sub> at 1400°C in air. *J Amer Ceram Soc.* 2001;84:1093–6. <https://doi.org/10.1111/jace.2001.84.issue-5>.

**Publisher's Note** Springer Nature remains neutral with regard to jurisdictional claims in published maps and institutional affiliations.